Available online at www.sciencedirect.com
ScienceDirect
Journal of the European Ceramic Society 31 (2011) 377–383
www.elsevier.com/locate/jeurceramsoc

Mullite crystallization kinetics of lanthanum doped sol–gel derived precursors

Stanislav Kurajica [a], Emilija Tkalcec [a,*], Vilko Mandic [a], Joerg Schmauch [b]

[a] *University of Zagreb, Faculty of Chemical Engineering and Technology, Marulicev trg 19, HR-10000 Zagreb, Croatia*
[b] *University of Saarland, FR 7 3, D-66041 Saarbruecken, Germany*

Received 15 June 2010; received in revised form 4 October 2010; accepted 11 October 2010
Available online 10 November 2010

Dedicated to the memory of our Professor, colleague and friend Aleksandar Bezjak.

Abstract

Kinetics of mullite crystallization of lanthanum-doped gels was studied under isothermal and non-isothermal conditions by using differential thermal analysis (DTA). The precursors for gel preparations are tetraethoxysilane, aluminum nitrate nonahydrate and lanthanum nitrate hexahydrate dissolved in ethanol. X-ray diffraction (XRD) and transmission electron microscopy (TEM) were used to identify the phase composition of samples. Prior to crystallization, the phase separation in two microphases occurs in the gels. The first microphase was alumina-rich and the second silica- and lanthanum-rich. The crystallization kinetics of mullite was influenced by the phase separation, which became more pronounced with an increasing amount of lanthanum. The phase separation reduced the incubation time and increased the Avrami exponent. The values of activation energy for mullitization slightly decreased with the increasing amount of lanthanum, due to the change in composition of the microphases from which mullite crystallized.

Keywords: Sol–gel process; Mullite; La doped precursors; Crystallization kinetics

1. Introduction

Mullite, $Al_2^{VI}(Al_{2+2x}^{IV}Si_{2-2x})O_{10-x}$, with x ranging between about 0.2 and 0.9, is widely used to produce both traditional and advanced ceramics, because of its favorable thermal and mechanical properties.[1]

Mullite crystallization on heating follows two different pathways in dependence on starting materials. From mixtures of kaolinite and alumina, sol mixtures and diphasic (colloidal) gels, mullite is formed above 1473 K via the metastable Al–Si spinel phase. From monophasic (polymeric) gels and glasses, mullite is formed directly at temperatures between 1173 and 1273 K.[2] Different mullitization routes are attributed to the different degree of mixing of the Al_2O_3 and SiO_2 precursors. In polymeric gels and glasses, the degree of mixing is on a molecular scale and consequently, the diffusion path length between Al and Si in the particles is short.

Extensive work has been done related to the crystallization kinetics of both groups of mullite precursor materials. A good review on crystallization kinetics and activation energies of mullitization from various starting materials was published recently by Okada.[3] Numerous researches, studying crystallization kinetics of mullite, reported that mullitization occurs via nucleation-growth mechanisms. There are, however, different opinions on the rate-controlling step of mullitization.[3] While the process of crystallization of less homogeneous precursors has been well investigated, insufficient data are available on the controlling step of mullitization from molecularly mixed precursors. The same stands for doped precursors of the two categories of mullite precursors.

The first investigation on mullite crystallization kinetics of monophasic precursor was presented by Li and Thompson,[4] with E_a values of 293 and 362 kJ mol^{-1}. It turned out later that these values were considerably smaller than those reported by other authors.[5–12] According to Li and Thompson, the controlling step for mullitization from the monophasic gel was nucleation. Tkalcec et al.[5] reported E_a values for mullitization of a monophasic gel to be 1053 kJ mol^{-1} and 1028 kJ mol^{-1},

* Corresponding author. Tel.: +385 1 4597 219; fax: +385 1 4597 260.
E-mail address: etkalcec@fkit.hr (E. Tkalcec).

0955-2219/$ – see front matter © 2010 Elsevier Ltd. All rights reserved.
doi:10.1016/j.jeurceramsoc.2010.10.017

with phase separation as the controlling step. Takei et al. studied the mullitization of glass fibers and ultra quenched glasses. The activation energy varied in the range of 1099–1195 kJ mol^{-1} for glass fibers[6] and 903–1133 kJ mol^{-1} for ultra quenched glasses.[7] They concluded that the mullitization process was nucleation controlled by diffusion of Si atoms in the amorphous matrix. Johnson et al.[8] found that crystallization of amorphous and quenched glass occurred in two steps, with E_a = 892 kJ mol^{-1} for the first step and 1333 kJ mol^{-1} for the second step. The combined average value of n was 3.23, indicating a three dimensional crystal growth. Okada *et al.*[9] reported E_a value of 1202 kJ mol^{-1} and diffusion as the rate-controlling step for mullite crystallization from polymeric xerogels. Douy[10] investigated the crystallization of amorphous precursor in whole composition range in the Al_2O_3–SiO_2 system and obtained E_a = 1395 kJ mol^{-1} for the stoichiometric 3:2 mullite composition, while lower values were obtained for non-stoichiometric precursors. Mullite as a sole phase crystallized from compositions with up to 70 mol.% Al_2O_3, spinel and mullite were found from compositions between 70 and 80 mol.% Al_2O_3, and only spinel was available from alumina-richer compositions. Leivo et al.[11] reported activation energies for crystallization of two mullite phases from monophasic gels to be 600–950 kJ mol^{-1} and 1120–1170 kJ mol^{-1} for the first and second mullite phases, respectively. The Avrami exponent was close to 1 for the first and above 3 for the second phase. Tan et al.[12] investigated activation energies of mullite fibers prepared from monophasic precursors. They obtained an E_a value of 741 kJ mol^{-1} and proposed phase separation to be the rate-controlling step.

Depending on the synthesis procedure, mullite is able to tolerate considerable amount of foreign cations,[13] however there are only a few reports examining the role of these cations in the mullitization of molecularly mixed precursors,[14] especially in crystallization kinetics. Mullite formation in the presence of lanthanum was recently investigated,[15–17] but to the best of our knowledge, crystallization kinetics of lanthanum doped pre-mullite gels has not been reported.

In this paper, mullite crystallization kinetics of monophasic precursors doped with various concentrations of lanthanum was studied under isothermal and non-isothermal conditions. The obtained kinetic parameters were discussed with respect to lanthanum concentrations and experimental conditions.

2. Experimental

The pre-mullite gel was prepared by dissolving $Al(NO_3)_3{\cdot}9H_2O$ (p.a., Kemika, Croatia) and $(La(NO_3)_3{\cdot}6H_2O$ (p.a., Kemika, Croatia) in ethanol (96% purity, Kemika, Croatia), the molar ratio of La to Al was 0, 1:100, 2:100 and 3:100 while the nitrate/ethanol molar ratio was 1:9. The solution was stirred and refluxed at 333 K for 1 day. Tetraethoxysilane (98% purity, Merck, Germany), which was mixed with ethanol (TEOS/ethanol molar ratio 1:9) and stirred at room temperature for 1 h, was added drop-wise to the nitrate solution. The ratio of Al to Si was 3:1, which corresponds to stoichiometric 3:2 mullite. The mixture was stirred under reflux conditions at 333 K for 8 days. The gel was dried under 150 W IR lamp for 1 day, further dried at 383 K for 3 days in a laboratory drier and then calcined in a laboratory furnace at 973 K for 2 h to decompose the organics and remove the volatiles. The calcined gel was manually crushed and ground in a corundum mortar, seized to particles smaller than 63 μm and stored in a desiccator. The samples were labeled according to the La to Al ratio as LM0 (without La), LM1 (La/Al = 1/100), LM2 (La/Al = 2/100) and LM3 (La/Al = 3/100).

Thermal behaviors of the powder precursors were characterized with Differential Thermal Analysis (Netzsch STA 409 analyzer). About 50 mg of powder was placed in Pt crucibles and heated at a rate of 10 K min^{-1} to 1623 K in a synthetic air flow of 30 cm^3 min^{-1}, α-alumina was used as a reference.

The samples were heated to 1273 K and analyzed by XRD using a Philips PW 1830 diffractometer with CuKα radiation. Data were collected between 5° and 70° 2θ in a step scan mode at a step of 0.02° and counting time of 2 s per step.

The amount of alumina in mullite was calculated from a linear dependence of the ratio of (2 2 0) and (1 1 1) mullite reflection intensities using the Ban and Okada relation[18]:

$$Al_2O_3\ (\text{mol.}\%) = 41.77\frac{I(2\,2\,0)}{I(1\,1\,1)} + 27.6 \quad (1)$$

Isothermal analyses were carried out at temperatures between 1223 and 1242 K and non-isothermal analyses were performed at five different heating rates (5, 7 10, 15 and 20 K min^{-1}).

In order to determine kinetic parameters under isothermal conditions, the appropriate differential function of the Johnson-Mehl-Avrami equation (Eq. (2)) was fitted to the shape of DTA curve[19]:

$$q\frac{d\alpha}{dt} = qnk^n(t-\tau)^{n-1}\exp[-k^n(t-\tau)^n] \quad (2)$$

$$k = k_0\exp\left[-\frac{E_a}{RT}\right] \quad (3)$$

where α is the volume fraction of crystallized mullite, the reaction kinetics was contained within the reaction constant, k, and it was related to the activation energy for the nucleation and growth process, E_a, through the Arrhenian temperature dependence (Eq. (3)). The dimensionless constant, n, is known as the Avrami exponent, which is related to nucleation and growth mechanisms, τ is related to transient time. The constant, q, is introduced in order to normalize the peak. Prior to fitting the baselines were subtracted from the original data. By doing so, parameters k, n and τ for each temperature were obtained. Subsequently, a plot of $\ln k$ *vs.* $1/T$ (Eq. (3)) was used to determine E_a for the crystallization process from the slope of the straight line.

The activation energy for mullite crystallization in non-isothermal conditions was calculated using the Kissinger–Akahira–Sunose method[20]:

$$\ln\left(\frac{\beta_i}{T_{\alpha i}^2}\right) = -\frac{E_a^{NG}}{RT_{\alpha i}} + C \quad (4)$$

where β_i is the heating rate, $T_{\alpha i}$ is the temperature corresponding to the degree of conversion α, E_α is the activation energy

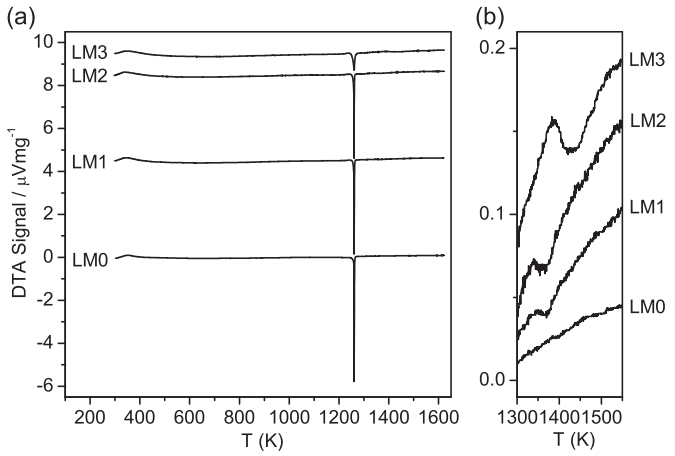

Fig. 1. (a) Non-isothermal DTA scans of the calcined LM0, LM1, LM2 and LM3 obtained at the heating rate of 10 K min^{-1}; (b) enlarged segment of the DTA curves in the temperature interval between 1300 and 1550 K. Scans are shifted for visualization purpose.

determined at the degree of conversion α, R is the universal gas constant and C is a constant. For seven degrees of conversion between $\alpha = 0.2$–0.8, a corresponding $T_{\alpha i}$ and heating rate were used to plot $\ln(\beta_i / T_{\alpha i}^2)$ against $1/T_{\alpha i}$. The plot should be a straight line whose slope can be used to calculate the activation energy, E_a.

The microstructure and morphology of the samples were examined by using transmission electron microscopy (TEM), TEM JEOL 2011, at an accelerating voltage of 200 kV, equipped with an energy dispersive X-ray spectrometer (EDX, Oxford LINK ISIS). The later was used for microanalysis of mullite grains and the glassy phase. TEM specimens were prepared by the typical ion-milling procedure using an ion-miller (PIPS 691 Gatan Co., USA).

3. Results and discussion

For a pure sample (LM0), only one sharp exothermic peak with maximum at 1261 K was observed (Fig. 1a). Such DTA scan is typical for monophasic gels having sufficient homogeneity for direct mullite formation below 1273 K.[21] For doped samples, besides the peak with maximum between 1260 and 1261 K, an additional broad peak in the range of 1340–1500 K was observed (Fig. 1b). Such a scan is characteristic of diphasic pre-mullite gels.[21] Although a slight variation in the first peak maxima is recorded, it is within error span. Therefore, it can be concluded that lanthanum doping does not affect crystallization temperature of the precursors. On the other hand, a decrease in peak height and an increase in peak width can be observed more and more obviously with increasing lanthanum loading. A decrease in peak area, particularly notable for LM3, is also seen. At the same time, intensity of the second peak increases and, for LM3, the peak shifts to higher temperatures. Such DTA peak features imply changes in crystallization mechanisms for the samples with different amounts of lanthanum.

XRD patterns of the samples are shown in Fig. 2. Mullite is a sole crystalline phase in the non-doped sample heated at 1273 K.

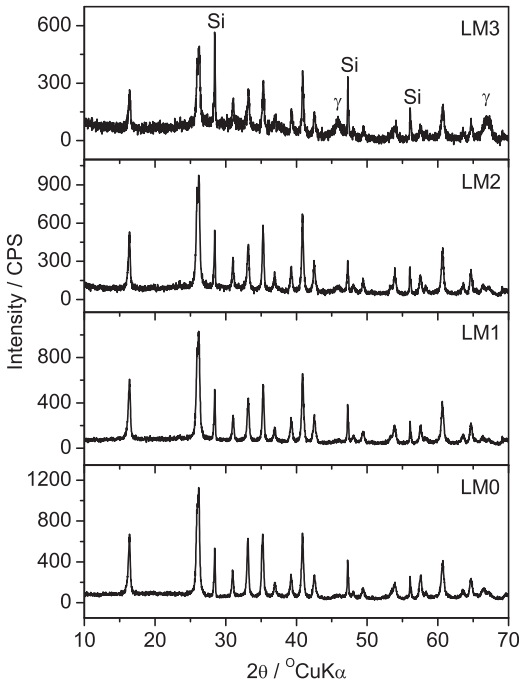

Fig. 2. XRD patterns of LM0, LM1, LM2 and LM3 calcined at 973 K for 2 h and heated to 1273 K. Si—silicon (internal standard). γ—γ-Al_2O_3. Mullite lines are not marked.

A considerable amount of γ-alumina, as a secondary crystalline phase, appears in LM3. In fact, most researches consider this phase as a solid solution of γ-alumina and silica.[22] Owing to its spinel-type structure, this phase is called Al–Si spinel. A small amount of Al–Si spinel also exists in samples LM1 and LM2, as shown by the weak and broad peaks at 46° and 67° 2θ. The Al–Si spinel in the samples transformed at higher temperatures to mullite, corresponding to the second exothermic DTA peak, as shown in Fig. 1b.

The overlapping of (1 2 0) and (2 1 0) mullite diffraction peaks clearly indicates that the so-called pseudotetragonal (alumina-rich) mullite has been obtained. This implies that at low temperatures mullite coexists with an amorphous silica-rich phase.[10]

The crystallization of alumina rich pseudotetragonal mullite rather than orthorhombic mullite in homogeneous molecular Al_2O_3–SiO_2 gels at 1253 K have been interpreted as a result of a phase separation prior to crystallization.[23] The same interpretation has been applied for mullite crystallization in rapidly quenched aluminosilicate glasses.[24] Huling and Messing[23] found that, for amorphous mullite gels and glasses, phase separation took place more rapidly than crystallization due to the high excess free energy of the homogeneous amorphous system. Molecular mobility and rearrangement are inherent aspects of heat treatment. As gels have to be calcined to remove volatiles prior to crystallization, this treatment provides an opportunity for phase separation.[23] Finally, spinel crystallization is induced as well as mullite if the local composition of heterogeneities exceeds 71 mol.% of Al_2O_3.[25]

Our previous investigations[26] have shown that either the amount of lanthanum incorporated into mullite lattice is neg-

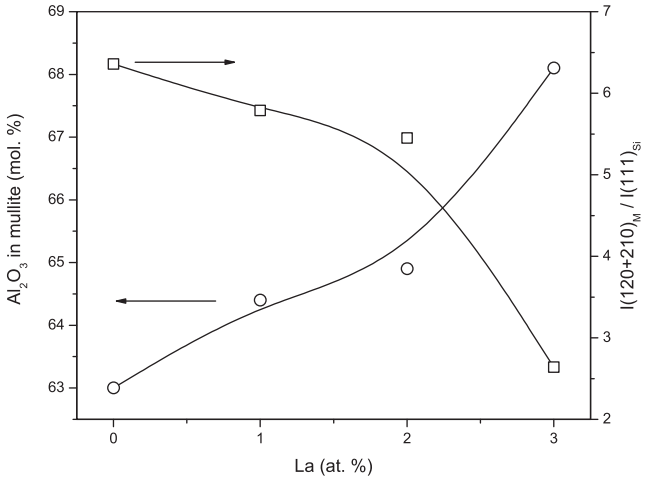

Fig. 3. Alumina content in mullite calculated using the Ban and Okada equation, and intensity ratio of (1 2 0 + 2 1 0) mullite to (1 1 1) silicon diffraction peak *vs.* lanthanum content. The lines are introduced as a guideline for the eye.

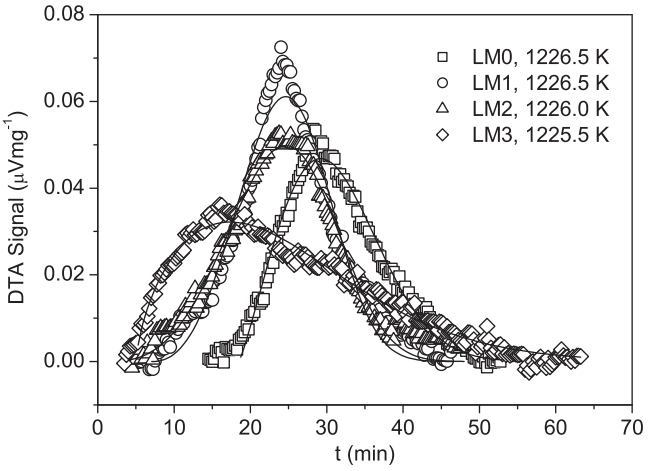

Fig. 4. Isothermal DTA scans of LM0, LM1, LM2 and LM3. The mean temperature value recorded during the mullite crystallization is expressed as the annealing temperature and given in the figure. The lines represent fits of Eq. (1) to experimental data.

ligible or lanthanum does not enter mullite crystal lattice at all. Therefore, structure parameters of mullite are affected only with Al_2O_3/SiO_2 ratio. In that case, the Ban and Okada relation (Eq. (1)) could be applied[18] to determine alumina content in mullite. Fig. 3 shows alumina content in mullite calculated by using the Ban and Okada equation. As can bee seen, mullite is richer in Al_2O_3 as lanthanum content is higher. Al_2O_3 content is 63.0 mol.% for LM0 and increases to 68.1 mol.% for LM3. A decrease of the amount of crystallized phase with the increase of lanthanum content was also observed. A relative quantity of mullite (represented by the ratio of the sum of intensities of (1 2 0) and (2 1 0) diffraction lines of mullite to (1 1 1) diffraction line of silicon ($I_{M(120)+(210)}/I_{Si(111)}$) as a function of lanthanum content is also shown in Fig. 3. The increase of Al_2O_3 content in mullite, as well as the decrease of mullite quantity, with the dopant concentration, implies an increase in the amorphous phase. The amorphous phase dominates in LM3, evidenced by the typical amorphous hump shown in Fig. 2. Since, neither crystalline lanthanum aluminate, nor lanthanum silicate were formed, La_2O_3 should be present in amorphous phase. La_2O_3 as a network modifier increases the number of non-bridging oxygen atoms in the amorphous structure, and consequently favors the diffusion and phase separation processes during the thermal treatment of the gels.[27] The localized compositional changes due to the phase separation ultimately preclude formation of stoichiometric mullite, but in favor of metastable alumina-rich mullite.

In order to obtain kinetic parameters, isothermal DSC scans of samples LM0, LM1, LM2 and LM3 obtained at different annealing temperatures in the range from 1223 to 1242 K were fitted to Eq. (2). Representative DTA curves and the corresponding fit lines are shown in Fig. 4. Obtained kinetic parameters are listed in Table 1.

The data of samples LM0, LM1 and LM2 represent only one nucleation and growth process. According to XRD patterns (Fig. 2), this is not the case for the sample LM3. Although, isothermal scans of sample LM3 could be fitted to one crystallization (nucleation and growth) process quite well, the data represents two crystallization processes: crystallization of mullite and Al–Si spinel. Such a crystallization path is a consequence of ultimately reduced homogeneity of the precursor. This is particularly visible in the values of the Avrami exponent, dramatically reduced for the sample LM3 with respect to other two doped samples.

The kinetic parameters, k, n and τ calculated using Eq. (2), are reported in Table 1. A significant difference in incubation time, which decreases with the amount of lanthanum, can be observed. While a transformation in LM0 was preceded by a notable incubation period, this effect is almost negligible for samples LM2 and LM3. The decrease in incubation time is obviously the consequence of the promotion of nucleation, most probably induced by the phase separation, and the process is more pronounced with a higher content of lanthanum. Takei et al. reported that the nucleation of mullite in glass was influenced by a phase separated texture formed prior to crystallization,[6] which might provided large interfaces favorable to the subsequent nucleation.[28] As argued before, phase separation into Al_2O_3-rich and SiO_2-rich regions, occurred in the samples prior to crystallization, which is more pronounced with higher content of lanthanum. Increased phase separation caused microstructure changes, i.e., the increase in interface to volume ratio. Phase boundaries have a lower thermodynamic barrier for nucleation of mullite and act as energetically favorable nucleation sites. Therefore, the decrease in the incubation period with the amount of lanthanum could be explained as a consequence of enhanced nucleation.

The value of the Avrami exponent, n, represents nucleation conditions, subsequent mechanism and the dimensionality of growth for which the data best fit the nucleation and growth model.[29] Ranganathan and von Heimendahl[30] suggested that Avrami exponent n can be expressed as: $n = p/s + q$, where p is the dimension of growth (with values 1, 2, or 3 for one-, two-, and three-dimensional growth, respectively), s is the growth index ($s = 1$ for interface-controlled growth and $s = 2$ for dif-

Table 1
Kinetic parameters for mullitization under isothermal conditions.

Sample	Temperature[a], T (K)	Rate constant, k (min^{-1})	Avrami exponent, n	Incubation time, τ (min)
LM0	1223.2	0.05	2.28	26
	1226.6	0.07	2.18	18.5
	1229.7	0.095	2.3	13
	1232.5	0.139	2.11	10
	1235.6	0.183	2.22	7
	1238.7	0.227	2.2	4.5
LM1	1223.4	0.04	3.53	8.5
	1226.3	0.051	3.44	7
	1229.1	0.068	3.49	5.5
	1232.4	0.091	3.58	3.5
	1235.1	0.11	3.56	2.5
	1237.9	0.157	3.58	2
	1241.3	0.235	3.56	1.5
LM2	1223.0	0.028	3.91	<1
	1225.9	0.039	3.85	<1
	1229.1	0.047	3.61	<1
	1232.4	0.065	3.44	<1
	1235.3	0.095	3.44	<1
	1238.1	0.116	3.49	<1
	1241.3	0.161	3.55	<1
LM3	1223.2	0.039	1.74	<1
	1225.3	0.045	1.62	<1
	1226.6	0.06	1.96	<1
	1230.1	0.082	1.69	<1
	1233.3	0.11	1.83	<1
	1236.8	0.14	1.85	<1
	1239.8	0.188	1.76	<1

[a] The mean temperature value recorded during the annealing.

fusion controlled growth), q is the nucleation index, which can range from 0 to >1 ($q = 0$ for a nucleation rate of zero, $0 < q < 1$ for a decreasing nucleation rate with time, $q = 1$ for a constant nucleation rate and $q > 1$ for an increasing nucleation rate). The values of Avrami exponents for the samples are listed in Table 1. By taking experimental errors into account, the Avrami exponents, n, for each sample are assumed constant for various annealing temperatures. The considerable increase in Avrami exponents for samples LM1 and LM2 with respect to the non-doped sample can be observed. Taking the Avrami exponent formalism[30] into account, the time exponent slightly higher than 2 for sample LM0 means the diffusion controlled three-dimensional growth, accompanied with an additional decreasing rate of nucleation. This is in accordance with the results reported by Okada et al.[9] who observed the diffusion controlled growth of mullite in an Al_2O_3-rich homogeneous polymeric gel. By the same formalism, Avrami exponents for samples LM1 and LM2 could be explained by the three-dimensional interface controlled growth, also accompanied by a decreasing rate of nucleation. The additional, decreasing rate of nucleation in the course of growth could be attributed to the bulk nucleation rather than to nucleation at the interfaces. It is therefore suggested that nucleation started from the interface and then additional nucleation coinciding with growth occurred within Al_2O_3 rich separated areas. As argued before, the Avrami exponent for sample LM3 is a consequence of two crystallization peaks overlapping, therefore it gives no relevant information about the crystallization mechanism of each phase.

Rate constants, k, are functions of temperature, and as expected, increase with annealing temperature. They are assumed to follow Arrhenius dependence. The Arrhenius plots for all four constant rate sets (Fig. 5) have a good linearity, which enabled calculation of activation energies. The plots were fitted by linear least squares regression to get the activation energies. The calculated values are presented in Fig. 6.

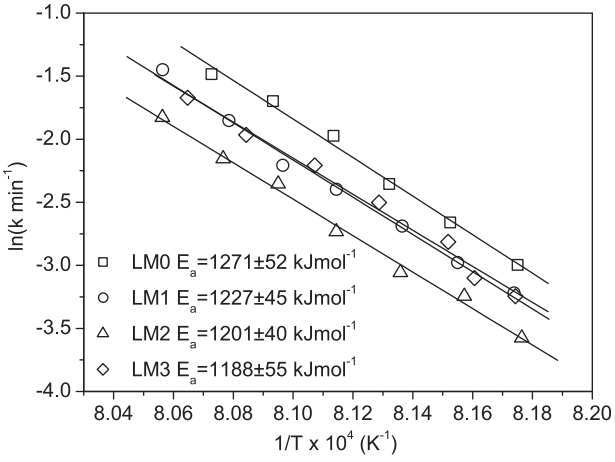

Fig. 5. Arrhenius plot of ln k *vs.* 1/T (rate constants k are given in Table 1).

Table 2
EDS analysis of the LM3 sample heat treated to 1873 K for 4 h.

Spot	O		Al		Si		La	
	(wt.%)	(mol.%)	(wt.%)	(mol.%)	(wt.%)	(mol.%)	(wt.%)	(mol.%)
Diffrac 1 (Mullite)	49.14	62.27	38.99	29.30	11.63	8.40	0.24	0.04
Diffrac 2 (Amorphous)	29.42	59.32	9.54	11.41	16.46	18.91	44.58	10.36

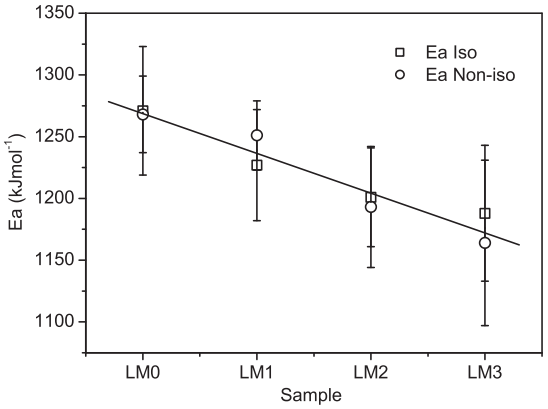

Fig. 6. Activation energies of mullitization determined under isothermal and non-isothermal conditions for LM0, LM1, LM2 and LM3.

The activation energies for crystallization were also determined in non-isothermal conditions by varying heating rate from 5 to 20 K min^{-1}. The results are also presented in Fig. 6. Remarkably good agreement of the values determined in both isothermal and non-isothermal conditions has been obtained.

Several values have been reported for the activation energies of mullite crystallization from precursors with a molecular level of homogeneity[5–12] and the values obtained in the present investigation are within the range of values reported. However, a decrease in activation energy with the increase of lanthanum content has been observed. As shown previously, the decreasing trend of E_a is attributed to the formation of Al-richer mullite. Recently, Douy[10] reported E_a for mullitization from monophasic gels with different chemical compositions. The maximum value was found for the precursor with 60 mol.% Al_2O_3, while E_a decreased significantly for the precursors with higher and lower alumina contents. The same dependence is noted by Okada.[3] In Al_2O_3 rich precursors, this is attributed to simultaneous crystallization of γ-Al_2O_3 and mullite, assuming that γ-Al_2O_3 has lower E_a than mullite and therefore it lowers the resulting average E_a values. Our results are in accordance with the statements above. In the sample LM0 no γ-Al_2O_3 was detected (Fig. 2), therefore the sample exhibited the highest activation energy. With the increase of lanthanum content, the amount of γ-Al_2O_3 in the sample increased, consequently the activation energy decreased as shown in Fig. 6.

TEM micrographs and corresponding selected area electron diffraction (SAED) of LM3 thermally treated at 1873 K are shown in Fig. 7. Besides mullite grains, a glassy phase in triple points was determined. The results of EDS analysis of amorphous and crystalline phase in the sample are summarized in Table 2. According to EDS analysis, the amount of Al_2O_3 in mullite was decreased to ~63.6 mol.%. The shift towards stoichiometric mullite comparing to previously determined composition through Ban and Okada relation is expected consequence of higher thermal treatment temperature. With the temperature increase a progressive decrease of initially high Al_2O_3 mullite content is generally observed, i.e., on further

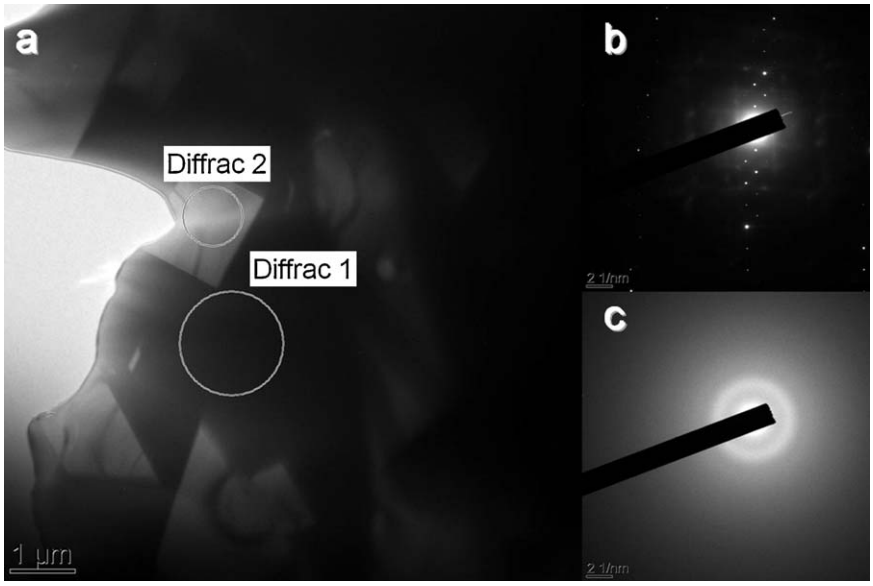

Fig. 7. (a) TEM bright field micrograph of LM3 heat treated at 1873 K for 4 h; (b) SAED pattern at position marked as Diffrac 1 (mullite); (c) SAED pattern at position marked as Diffrac 2 (glassy phase).

heating alumina-rich mullite evolves to a composition near to $3Al_2O_3{\cdot}2SiO_2$.[10] The traces of lanthanum in mullite are most likely attributable to X-ray emission from the neighboring La_2O_3 rich glassy phase[17] or glass contained in pores of mullite grain. As expected, the glassy phase is rich on silicon and lanthanum.

4. Conclusion

Crystallization kinetics of monophasic mullite doped with lanthanum has been investigated in isothermal and non-isothermal conditions.

Prior to crystallization a phase separation occurred in the gels. Two separated microphases emerged, one was richer in alumina and almost completely depleted of lanthanum and the other was richer in silica containing almost all lanthanum. The greater the quantity of lanthanum in the sample, the more pronounced is the phase separation and the richer in Al_2O_3 is the later crystallized mullite.

The phase separation influenced the crystallization kinetics of mullite. The increased phase separation reduced the incubation time due to a nucleation of mullite on interface, and increased the Avrami exponent due to the change of the growth controlling mechanism. The activation energy for mullitization slightly decreased with the amount of lanthanum due to changes in the composition of the microphase, from which mullite crystallizes.

Acknowledgement

The financial support of the Ministry of Science, Education and Sports of Republic of Croatia within the framework of the project No. 125-1252970-2981 is gratefully acknowledged.

References

1. Schneider H, Schreuer J, Hildmann B. Structure and properties of mullite—a review. *J Eur Ceram Soc* 2008;**28**:329–44.
2. Okada K, Otsuka N, Somiya S. Review of mullite synthesis routes in Japan. *Am Ceram Soc Bull* 1991;**70**:1633–40.
3. Okada K. Activation energy of mullitization from various starting materials. *J Eur Ceram Soc* 2008;**28**:377–82.
4. Li DX, Thomson WJ. Mullite formation kinetics of a single-phase gel. *J Am Ceram Soc* 1990;**73**:964–9.
5. Nass R, Tkalcec E, Schmauch J, Schmidt H, Kurajica S, Bezjak A, et al. Crystallization kinetics of mullite from single-phase gel determined by isothermal differential scanning calorimetry. *J Non-Cryst Solids* 1998;**223**:57–72.
6. Takei T, Kameshima Y, Yasumori A, Okada K. Crystallization kinetics of mullite in alumina–silica glass fibers. *J Am Ceram Soc* 1999;**82**:2876–80.
7. Takei T, Kameshima Y, Yasumori A, Okada K. Crystallization kinetics of mullite from Al_2O_3–SiO_2 glasses under non-isothermal conditions. *J Eur Ceram Soc* 2001;**21**:2487–93.
8. Johnson BR, Kriven WM, Schneider J. Crystal structure development during devitrification of quenched mullite. *J Eur Ceram Soc* 2001;**21**:2541–62.
9. Okada K, Kaneda J, Kameshima Y, Yasumori A, Takei T. Crystallization kinetics of mullite from polymeric Al_2O_3–SiO_2 xerogels. *Mater Lett* 2003;**57**:3155–9.
10. Douy A. Crystallization of amorphous spray-dried precursors in the Al_2O_3–SiO_2 system. *J Eur Ceram Soc* 2006;**26**:1447–54.
11. Leivo J, Lindén M, Ritola M, Vippola M, Levänen E, Mäntylä TA. Influence of thermal treatment conditions on the formation of phase-pure mullite derived from a nanoparticulate aluminosilicate precursor. *Mater Chem Phys* 2009;**115**:56–64.
12. Tan H, Ding Y, Yang J. Mullite fibres preparation by aqueous sol–gel process and activation energy of mullitization. *J Alloys Compd* 2009;**492**:396–401.
13. Schneider H. Transition metal distribution in mullite. In: Somiya S, Davis RF, Pask JA, editors. *Ceramic transactions, vol. 6, mullite and mullite matrix composites*. Westerville: American ceramic Society; 1990. p. 135–57.
14. Okada K, Otsuka N. Formation processes of mullite. In: Somiya S, Davis RF, Pask JA, editors. *Ceramic transactions, vol. 6, mullite and mullite matrix composites*. Westerville: American ceramic Society; 1990. p. 375–87.
15. Ferreira de Souza M. Nucleation and growth of mullite whiskers from lanthanum-doped aluminosilicate melts. *J Am Ceram Soc* 2002;**85**: 232–8.
16. Kong LB, Zhang TS, Ma J, Boey F, Zhang RF. Mullite phase formation in oxide mixtures with the presence of Y_2O_3, La_2O_3 and CeO_2. *J Alloys Compd* 2004;**372**:290–9.
17. Regiani I, Magalhaes WLE, Ferreira de Souza DP, Paiva-Santos CO, Ferreira de Souza M. Nucleation and growth of mullite whiskers from lanthanum-doped aluminosilicate melts. *J Am Ceram Soc* 2002;**85**: 232–8.
18. Ban T, Okada K. Structure refinement of mullite by the Rietveld method and a new method for estimation of chemical composition. *J Am Ceram Soc* 1992;**75**:227–30.
19. Kurajica S, Bezjak A, Tkalcec E. Resolution of overlapping peaks and the determination of kinetic parameters for the crystallization of multicomponent system from DTA or DSC curves: II. Isothermal kinetics. *Thermochim Acta* 2000;**360**:63–70.
20. Akahira T, Sunose T. Method of determining activation deterioration constant of electrical insulating materials. *Research Report, Chiba Inst Technol* 1971;**16**:22–3.
21. Schneider H, Saruhan B, Voll D, Merwin I, Sebald A. Mullite precursor phases. *J Eur Ceram Soc* 1993;**11**:87–94.
22. Tkalcec E, Kurajica S, Ivankovic H. Diphasic aluminosilicate gels with two stage mullitization in temperature range of 1200–1300 °C. *J Eur Ceram Soc* 2005;**25**:613–26.
23. Hulling JC, Messing GL. Chemistry-crystallization relations in molecular mullite gels. *J Non-Cryst Solids* 1992;**147–148**:213–21.
24. Risbud SH. Revisiting metastable immiscibility and structure in silica-alumina glasses. In: Somiya S, Davis RF, Pask JA, editors. *Ceramic transactions, vol. 6, mullite and mullite matrix composites*. Westerville: American ceramic Society; 1990. p. 61–71.
25. Parmentier J, Vilminot S. Influence of synthesis and composition on mullite crystallization. *Chem Mater* 1997;**9**:1134–7.
26. Mandic V, Tkalcec E, Kurajica S. The influence of La_2O_3 on sol–gel derived mullite densification behavior. In: Nasr M, editor. *Proceedings of MTM2008*. Kairo: CMRDI; 2008.
27. Iftekhar S, Grins J, Eden M. Composition-property relationships of the La_2O_3–Al_2O_3–SiO_2 glass system. *J Non-Cryst Solids* 2010;**356**:1043–8.
28. Takei T, Kameshima Y, Yasumori A, Okada K. Calculation of metastable immiscibility region in the Al_2O_3–SiO_2 system using molecular dynamics simulation. *J Mater Res* 2000;**15**:186–93.
29. Christian JW. *The theory of transformations in metals and alloys, Part I: equilibrium and general kinetics theory*. 3rd ed. Oxford: Elsevier; 2002. p. 529–52.
30. Ranganathan S, von Heimendahl M. The three activation energies with isothermal transformations: applications to metallic glasses. *J Mater Sci* 1981;**16**:2401–4.